crystals

MDPI

Article

Influence of Defects in Boron Nitride Nanotubes in the Adsorption of Molecules. Insights from B3LYP-D2* Periodic Simulations

Oriol Matarín and Albert Rimola *

Departament de Química, Universitat Autònoma de Barcelona, 08193 Bellaterra, Spain; oriol.matarin@gmail.com
* Correspondence: albert.rimola@uab.cat; Tel.: +34-935-812-164

Academic Editors: Umit B. Demirci, Philippe Miele and Pascal G. Yot
Received: 27 April 2016; Accepted: 12 May 2016; Published: 20 May 2016

Abstract: The adsorption of H_2O, NH_3 and HCOOH as polar molecules and C_6H_6 and CH_4 as non-polar ones on a series of zig-zag (6,0) single-walled boron nitride nanotubes (BNNTs) both being defect-free (P_BNNT) and containing defects at the nanotube walls has been studied by means of B3LYP-D2* periodic calculations. We focused on defects derived from monovacancies of B (N-rich_BNNT) and N (B-rich_BNNT) atoms and also on Stone-Wales defects (SW_BNNT). The adsorption of polar molecules with defective BNNTs is generally based on dative interactions and H-bonding, and their adsorption energies strongly depend on the type of BNNT. N-rich_BNNT is the most reactive nanotube towards adsorption of polar molecules, as in all cases deprotonation of the polar molecules is spontaneously given upon adsorption. The strength in the adsorption energies is followed by B-rich_BNNT, SW_BNNT and P_BNNT. Adsorption of non-polar molecules is mainly dictated by dispersion interactions, and, accordingly, the adsorption energies are almost constant for a given molecule irrespective of the type of nanotube.

Keywords: DFT; periodic simulations; boron nitride nanotubes; vacancies; Stone-Wales defect; adsorption

1. Introduction

Boron nitride nanotubes (BNNTs) are isosteres and structurally similar to carbon nanotubes (CNTs), in which alternating B and N substitute for C atoms. BNNTs were first theoretically predicted in 1994 [1,2] and then successfully synthesized in 1995 [3] by adopting various techniques for the growth of CNTs. BNNTs are electrical insulators with an almost constant band gap of *ca.* 5.5 eV, which is practically independent of their morphology, diameter, helicity and concentric layers. This is at variance with CNTs, which exhibit metallic or semiconducting characters, which in turn strongly depend on the tubular geometry features.

BNNTs possess attractive physical and chemical properties; *i.e.*, high chemical stability, high oxidation resistance, excellent mechanical properties and high thermal conductivity, that render them as appropriate candidates to be used as functional composites [4], nanoinsulating covers [5], gas accumulators [6,7], and can be valuable nanodevices working in hazardous and extreme environments. Excellent recent reviews focused on the structure, synthesis and applications of BNNTs are available [8–10]. However, the stable band gap and the low reactivity towards molecule adsorption (which essentially takes place via physisorption) may impose some limitations for extensive applications of BNNTs, for instance, as nanoelectro-optical devices. Thus, modifying its electronic and structural properties has a potential impact on these additional applications. One effective way to achieve this goal is to introduce defects at the BNNT walls, which in turn are inevitable in reality. Indeed, BNNTs are not defect-free absolutely. The conditions under which BNNTs are

synthesized (e.g., arc-discharge, laser ablation and chemical vapor deposition) can certainly promote the appearance of native defects. There are different classes of defects: (i) those related to substitutional impurities; *i.e.*, C, Si or O atoms substitute the natural B and N atoms; (ii) those related to the presence of vacancies, which can be monovacancies and divacancies; (iii) antisite substitutions, in which adjacent B and N atoms exchange postions; and (iv) Stone-Wales defects [11], a topological defect involving a change in the connectivity of a B-N pair due to a rotation of the midpoint of the pair. Some of them have been identified experimentally [12,13].

Several theoretical investigations have studied the physico-chemical features of defective BNNTs, in particular those related to vacancies and Stone-Wales defects [12,14–22]. These works were generally focused on the geometries, formation energies, electronic properties and reactivity of BNNTs containing Stone-Wales defects and vacancies. The presence of Stone-Wales defects induces a slight band gap reduction, whereas the presence of vacancies dramatically reduce the band gap, in which in some cases render the nanotubes as conductors. Reactivity near the defects is higher than that in perfect BNNTs; *i.e.*, the adsorption energies of small molecules is larger, in which, in some cases, molecule dissociation takes place upon adsorption on the defective sites.

To the best of our knowledge, adsorption and surface reactivity on defective BNNTs has exclusively been studied for their interaction with H_2, O_2, CO, H_2O and NH_3 as probe molecules, in which, moreover, different structural models for BNNTs and different DFT methods were employed. The purpose of this work is to present a comprehensive theoretical study based on periodic B3LYP-D2* calculations on the adsorption of different polar (H_2O, NH_3 and HCOOH) and non-polar (C_6H_6 and CH_4) probe molecules on zig-zag (6,0) single-walled BNNTs that contain Stone-Wales defects and boron and nitrogen monovacancies. A comparison of the adsorption of the probe molecules between defective and perfect BNNTs is also provided, which allows us to disentangle the influence of BNNT wall defects in surface reactivity.

2. Results and Discussion

2.1. Models for Perfect and Defective BNNTs

Figure 1 shows the periodic models of the BNNT structures used in this work. P_BNNT refers to a defect-free (*i.e.*, perfect) (6,0) BNNT with its regular hexagonal arrangements. SW_BNNT refers to the nanotube that contains Stone-Wales (SW) defect. SW defects are topological irregularities in which a given B-N bond rotates 90 degrees, converting the four adjacent six member rings of a pyrene-like region into two pentagon/heptagon pairs (with notation 5-7-7-5). Theoretical calculations point out that the 5-7-7-5 SW arrangements, despite having homoelemental B-B and N-N bonds, are more favorable than the 4-8-8-4 alternatives [23]. The 5-7-7-5 SW arrangement modelled in the present work has been reported as that requiring the lowest formation energy among different 5-7-7-5 possibilities [17]. N-rich_BNNT refers to a BNNT that presents a vacancy due to the removal of one B atom from the perfect BNNT. Structural reconstruction undergone by the N-rich_BNNT upon geometry optimization leads to the formation of an N–N bond, giving rise to a pentagon/nonagon pair. Interestingly, the nine-member ring contains a divalent N atom significantly exposed to an outermost position of the external wall (labeled by an asterisk), which may exhibit a significant basic character. Finally, B-rich_BNNT refers to a BNNT with the vacancy of one N atom; *i.e.*, one N atom was removed from the perfect BNNT. Geometry reconstruction of the B-rich_BNNT brings associated with a B-B bond formation, thus resulting in the formation of a pentagon/nonagon pair. Remarkably, the optimized geometry of the B-rich_BNNT has a coordinatively unsaturated B atom (labeled by an asterisk) very exposed to the BNNT walls, which may be a strong Lewis site.

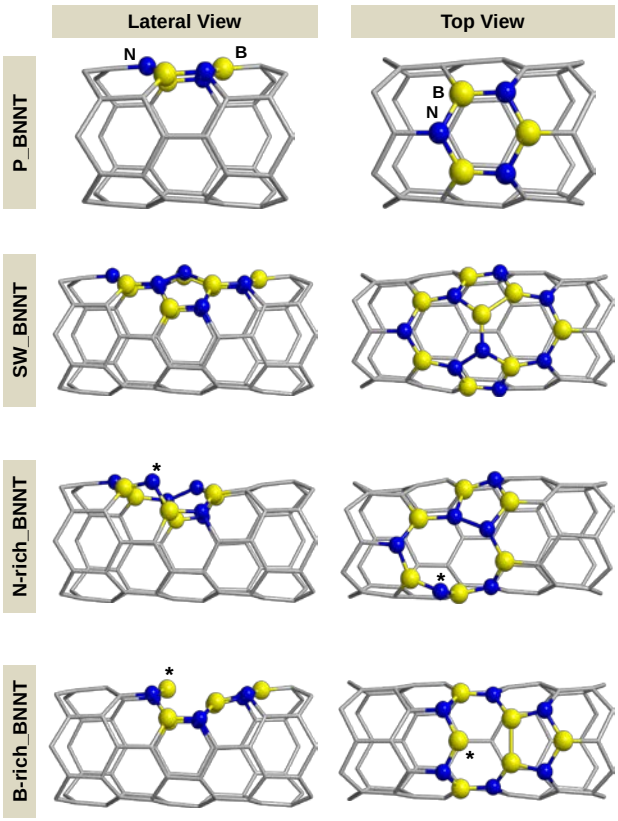

Figure 1. Lateral and top views of the different zig-zag (6,0) boron nitride nanotubes (BNNTs) used in this work: defect-free (P_BNNT); with a Stone-Wales defect (SW_BNNT); with a boron monovacancy (N-rich_BNNT); and with a nitrogen monovacancy (B-rich_BNNT). N-rich_BNNT exhibits an N atom very exposed to the BNNT wall and B-rich_BNNT a coordinatively unsaturated B atom, which are highlighted with an asterisk (see text).

The presence of these defects induces dramatic changes in the electronic properties with respect to the perfect BNNT. The calculated direct band gap of the perfect (6,0) BNNT is 4.42 eV, of the SW_BNNT is slightly lower; *i.e.*, 4.38 eV, whereas both the N-rich and the B-rich BNNTs are metallic; namely, there is an overlap between their valence and conduction bands. These electronic variations were already reported in previous theoretical works [12,14,17,22].

2.2. Features on the Adsorption of Probe Molecules

2.2.1. On P_BNNT

Figure 2 shows the B3LYP-D2* optimized geometries of the probe molecules in interaction with P_BNNT. Table 1 reports the calculated adsorption energies (ΔE_{ads}), including the contribution of the pure potential energies (ΔU) and the contribution of the dispersion interactions (ΔE_D) to the total ΔEads, and also the calculated Mulliken charges (Q) and the direct band gap (E_g) of the adducts. These data were already reported by some of us [24].

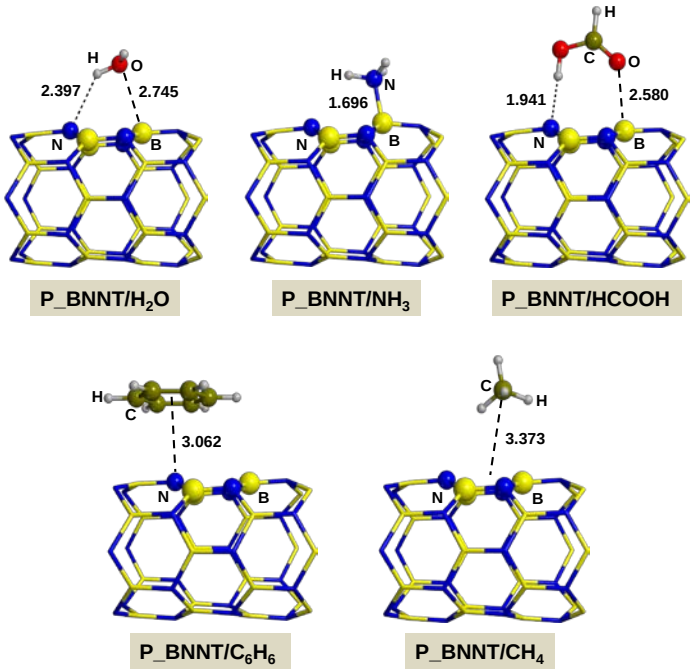

Figure 2. B3LYP-D2* optimized structures of the probe molecules interacting with P_ BNNT. Bond distances are in Å. The distances for P_BNNT/C_6H_6 are those between the centroid of the aromatic ring and the plane defined by the closest BN hexagon ring; for CH_4, they are between the C atom and the plane defined by the closest BN hexagon ring.

Table 1. Calculated adsorption energies (ΔE_{ads}), including the pure potential energy contribution (ΔU) and the contribution of dispersion (ΔE_D), of the probe molecules on the different BNNTs. The calculated Mulliken charges (Q) of the probe molecules adsorbed on the BNNTs, and calculated direct band gaps (E_g) of the adducts are also included.

Complex	ΔU	ΔE_D	ΔE_{ads}	Q (e)	E_g (eV)[2]
P_BNNT/H_2O	−2.3	−3.6	−5.9	0.03	4.41
P_BNNT/NH_3	−10.5	−5.1	−15.6	0.29	4.45
P_BNNT/HCOOH	−3.5	−5.5	−9.0	−0.03	4.42
P_BNNT/C_6H_6	+3.8	−12.8	−9.0	−0.02	4.40
P_BNNT/CH_4	+1.0	−4.0	−3.0	−0.02	4.42
SW_BNNT/H_2O	−2.4	−3.3	−5.7	−0.01	4.36
SW_BNNT/NH_3	−14.1	−4.4	−18.5	0.33	4.02
SW_BNNT/HCOOH	−5.8	−5.7	−8.5	0.17	4.08
SW_BNNT/C_6H_6	+3.6	−12.1	−8.5	−0.02	4.36
SW_BNNT/CH_4	+1.3	−4.1	−2.8	−0.02	4.37
N-rich_BNNT/H_2O	−93.7	−0.4	−94.1	−0.13[1]	conductor
N-rich _BNNT/NH_3	−86.7	−1.3	−88.0	−0.05[1]	conductor
N-rich _BNNT/HCOOH	−84.9	−4.0	−88.9	−0.23[1]	conductor
N-rich _BNNT/C_6H_6	+3.6	−13.1	−9.5	0.03	conductor
N-rich _BNNT/CH_4	+0.9	−4.0	−3.1	−0.03	conductor
B-rich_BNNT/H_2O	−12.0	−3.8	−15.8	0.31	conductor
B-rich _BNNT/NH_3	−28.7	−5.2	−33.9	0.41	conductor
B-rich _BNNT/HCOOH	−23.5	−7.5	−31.0	−0.22 [1]	conductor
B-rich _BNNT/C_6H_6	+3.2	−12.6	−9.4	0.03	conductor
B-rich _BNNT/CH_4	+1.0	−3.7	−2.7	−0.01	conductor

[1] In these complexes the acidic proton of the probe molecule is transferred to the BNNTs, and accordingly Q has been obtained with the calculated Mulliken charges of the atoms of the deprotonated anions. [2] The calculated band gap of the bare (6,0) P_BNNT is 4.42 eV, of the bare (6,0) SW_BNNT is 4.38 eV, and the bare (6,0) N-rich_BNNT and B-rich_BNNTs are conductors.

Among the polar molecules, the most stable adduct is P_BNNT/NH_3 (ΔE_{ads} = −15.6 kcal· mol^{-1}). It presents a covalent dative bond between a B atom of the nanotube and the N of NH_3. Analysis of the Q values indicate a charge transfer from NH_3 to P_BNNT of 0.29 *e* (see Table 1), thus confirming the dative nature of the interaction. This complex is energetically followed by P_BNNT/HCOOH and P_BNNT/H_2O (ΔE_{ads} = −9.0 and −5.9 kcal· mol^{-1}, respectively). Both systems are based on dispersive forces and also on weak dative and hydrogen-bond (H-bond) interactions, which, according to the calculated ΔE_{ads} values and the optimized structural parameters in P_BNNT/H_2O, are weaker than in P_BNNT/HCOOH.

The adsorption of C_6H_6 on P_BNNT is more favorable than CH_4 (ΔE_{ads} = −9.0 and −5.9 kcal mol^{-1}, respectively). For these cases, the adsorption mechanism is essentially dictated by dispersion interactions. The intermolecular distances (about 3 Å) are also consistent with an interaction driven by dispersion. Dispersion forces are stronger in P_BNNT/C_6H_6 than in P_BNNT/CH_4 because, in the former, the interaction is via a π-stacking mechanism, while in the latter through a CH-π mechanism. The calculated ΔU values are in both cases positive, so these complexes are stable due exclusively to dispersion (the ΔE_D values are negative, see Table 1).

For all the computed complexes, the interaction of the molecules does not induce any modification to the band gap of P_BNNT; *i.e.*, it remains almost unaltered, in agreement with the robust band gaps exhibited by perfect BNNTs.

2.2.2. On SW_BNNT

Figure 3 shows the complexes formed when the probe molecules interact with SW_BNNTs, and Table 1 reports the calculated adsorption energies and their contributions, and the calculated Q and E_g values.

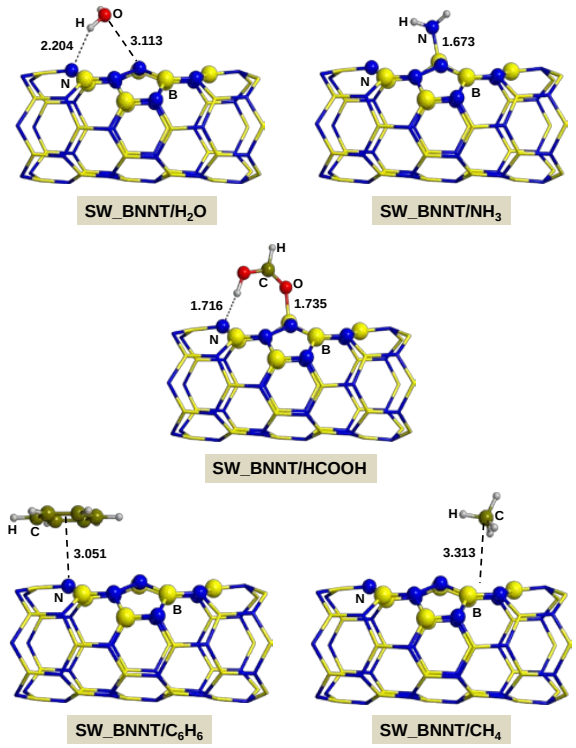

Figure 3. B3LYP-D2* optimized structures of the probe molecules interacting with SW_ BNNT. Bond distances are in Å. The distances for SW_BNNT/C_6H_6 are that between the centroid of the aromatic ring and the plane defined by the closest BN heptagon ring; for CH_4, they are between the C atom and the plane defined by the closest BN heptagon ring.

The geometry features of the SW_BNNT/NH_3 are similar to those for P_BNNT/NH_3; *i.e.*, NH_3 adsorbs on SW_BNNT with dative interactions, in which a $B_{(BNNT)}$-$N_{(NH3)}$ covalent bond is established. The interaction of HCOOH with SW_BNNT (the SW_BNNT/HCOOH complex) is also due to a dative bond, in this case between the CO group of HCOOH and a B atom of the nanotube, and also to an H–bond between the OH of HCOOH and an N atom of the nanotube. Accordingly, the nature of the adsorption of HCOOH on SW_BNNT is different to on P_BNNT, as in the latter case dispersion is the main adsorption mechanism. In contrast, H_2O adsorption on SW_BNNT is similar to that on P_BNNT; *i.e.*, dative and H-bond interactions are actually weak ($\Delta U = -2.4$ kcal mol^{-1}). The calculated adsorption energies are in agreement with all features; *i.e.*, SW_BNNT/NH_3 presents the most favorable adsorption energies, which are followed by SW_BNNT/HCOOH and SW_BNNT/H_2O ($\Delta E_{ads} = -18.5$, -11.5 and -5.7 kcal mol^{-1}, respectively). These values also indicate that the interaction of NH_3 and HCOOH on the SW defects is somewhat more favorable than when interacting with P_BNNT (about 2–3 kcal mol^{-1} more stable), which is mainly due to a more favorable ΔU term. The calculated charges also point out in this direction (Q values are larger in in the SW_BNNT complexes than in the P_BNNT complexes, see Table 1). However, this is not applicable to H_2O interaction. The calculated ΔE_{ads} values are similar in SW_BNNT/H_2O and P_BNNT/H_2O, with similar ΔU and ΔE_D contributions. Thus, presence of SW defects does not affect the adsorption of one water molecule, probably due to the low donor electron character of the O atom of H_2O upon BNNT adsorption.

Adsorption of C_6H_6 and CH_4 on SW_BNNT takes place through dispersion forces, and, accordingly, the structures and energetics of the SW_BNNT/C_6H_6 and SW_BNNT/CH_4 adducts are similar to the P_BNNT-analogues. That is, the adsorption of C_6H_6 takes place via π-stacking interactions and of CH_4 via CH-π interactions. Accordingly, the former molecule presents more favorable ΔE_{ads} values than the latter one (-8.5 and -2.8 kcal mol^{-1}), which in turn are very similar to the corresponding P_BNNT-analogue complexes.

For all adducts, the interaction of these molecules induces a slight decrease of the band gap of the SW_BNNT. The largest decrease is given by the most interacting molecules; *i.e.*, upon NH_3 and HCOOH adsorption (a reduction of about 0.36 and 0.30 eV, respectively), while for the other molecules the reduction is of about 0.02 eV (see Table 1).

2.2.3. On N-rich_BNNT

The optimized structures of the complexes formed by interaction of the probe molecules with the N-rich_BNNT model are shown in Figure 4, whereas Table 1 reports their energetic features and the calculated Q and E_g values.

All of the polar molecules interacting with this defective nanotube have a common feature: they become deprotoned species upon adsorption (see N-rich_BNNT/H_2O, N-rich_BNNT/NH_3 and N-rich_BNNT/HCOOH). Indeed, the direct interaction between the polar molecules and the nanotube takes place between the O (H_2O), N (NH_3) and CO (HCOOH) donor electron moieties and the B atom through a dative covalent bond. The interaction is also associated with a large charge transfer, which promotes a significant increase of the acidity of the protons of the molecules. These acidic-enhanced protons are close to a very basic N atom exposed to the wall of the nanotube (see above), and, during the geometry optimization process, a spontaneous proton transfer from the polar molecules to this N atom takes place. For these systems, Q values were calculated considering the atoms of the anionic species (*i.e.*, OH^-, NH_2^- and $HCOO^-$), which for all the cases are negative, thus attesting to a net charge transfer from the anionic species to the nanotube and indicating that electrostatic interactions are also operating in the binding mechanism. Proton transfers of this kind have also been reported in other works [24–26]. The calculated adsorption energies are large and very negative (they are indeed the most favorable ones presented in this work), which arise essentially from the ΔU potential energy contribution (dispersion contribution is almost residual, see Table 1). Interaction of N-rich_BNNT with H_2O gives the most stable adduct ($\Delta E_{ads} = -94.1$ kcal$\cdot$ mol^{-1}), which is followed by interaction

with HCOOH and NH_3, which in turn exhibit similar stabilities (ΔE_{ads} = −88.9 and −88.0 kcal· mol^{-1}, respectively).

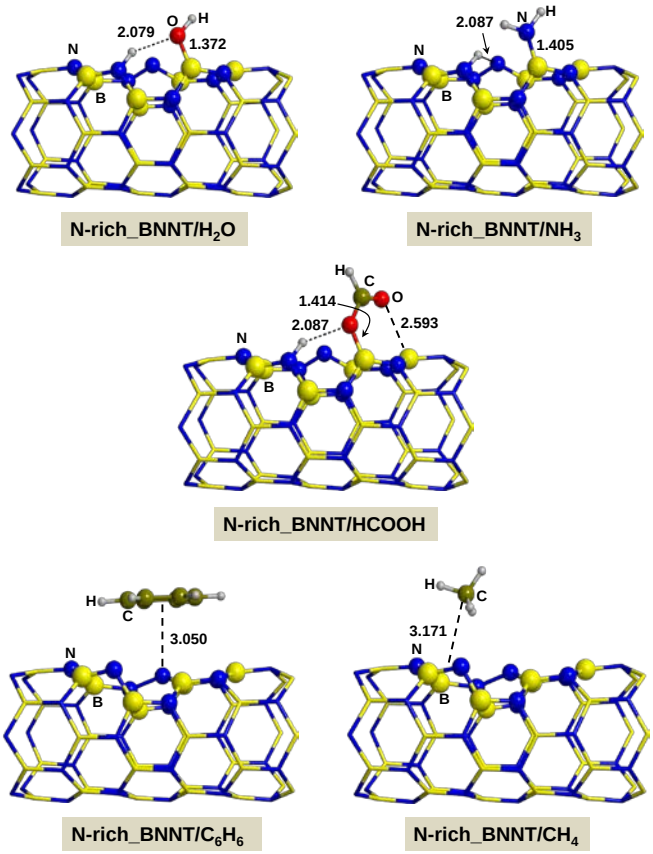

Figure 4. B3LYP-D2* optimized structures of the probe molecules interacting with N-rich_BNNT. Bond distances are in Å. The distances for N-rich_BNNT/C_6H_6 are those between the centroid of the aromatic ring and the plane defined by the closest nonagon ring; for CH_4, they are between the C atom and the plane defined by the closest nonagon ring.

The interaction of the non-polar molecules with N-rich_BNNT is completely different to that with the polar molecules. As C_6H_6 and CH_4 do not contain donor electron groups and acidic protons, neither dative interactions nor proton transfers processes occur in the adduct formation. The interaction is mainly driven by dispersion so the calculated adsorption energies (ΔE_{ads} = −9.4 and −2.7 kcal· mol^{-1} for N-rich_BNNT/C_6H_6 and N-rich_BNNT/CH_4, respectively) and the structural features (intermolecular distances of 3.050 and 3.171 Å, respectively) are very similar to the P_BNNT-analogue and SW_BNNT-analogue systems.

2.2.4. On B-rich_BNNT

As mentioned in Section 2.2.1, the B-rich_BNNT model has a coordinatively unsaturated B atom very exposed to the wall of the BNNT, and, accordingly, the polar molecules are expected to interact through this B atom. The initial guess structures adopted this structural feature and the systems collapsed onto the structures shown in Figure 5. Table 1 reports their energetic features, and the calculated Q and E_g values. The B-rich_BNNT/H_2O and B-rich_BNNT/NH_3 complexes have the H_2O and NH_3 molecules molecularly adsorbed on the B-rich_BNNT by means of a dative covalent bond between the O and the N atoms of the probe molecules and the exposed B atom. The calculated ΔE_{ads} values of these two complexes are largely more favorable than those of the P_BNNT-analogue and SW_BNNT-analogue complexes (−15.8 and −33.9 kcal mol^{-1}, respectively) because

the dative interactions are stronger in the B-rich_BNNT-analogue complexes (shown by the more favorable ΔU contributions), but less favorable than the N-rich_BNNT-analogues. Adsorption of HCOOH also presents a covalent dative bond, in this case between the CO group and the exposed B atom. In this adduct, however, the interaction leads to a spontaneous proton transfer from the HCOOH to the N atom of the nanotube, similarly to what occurs in the N-rich_BNNT/polar molecule complexes. The calculated adsorption energy is −31.0 kcal mol^{-1}, which is close to that for the B-rich_BNNT/NH_3 complex.

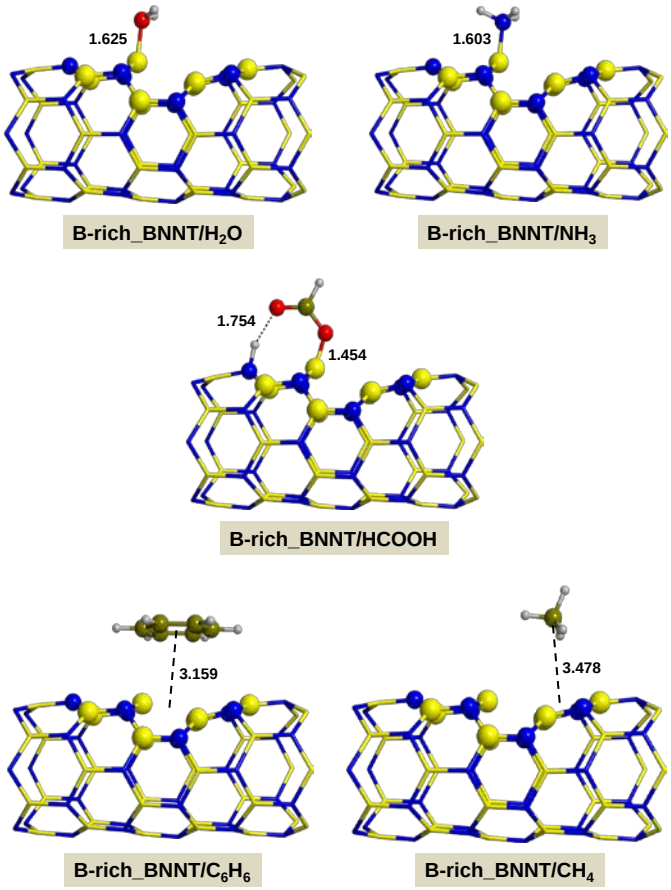

Figure 5. B3LYP-D2* optimized structures of the probe molecules interacting with B-rich_BNNT. Bond distances are in Å. The distances for B-rich_BNNT/C_6H_6 are those between the centroid of the aromatic ring and the plane defined by the closest nonagon ring; for CH_4, they are between the C atom and the plane defined by the closest pentagon ring.

The initial guess interaction of C_6H_6 with B-rich_BNNT also adopted a bond between the exposed B atom and the aromatic cloud of C_6H_6. However, the system, upon geometry optimization, evolved onto B-rich_BNNT/C_6H_6, in which this initial interaction is missed. The complex is stable due to dispersion interactions and accordingly the structural and energetic features are similar to those of the other C_6H_6-adsorbed complexes, with ΔE_{ads} = −9.4 kcal· mol^{-1}. B-rich_BNNT/CH_4 is also a dispersion-based adduct, which presents similar features to those of the other CH_4-adsorbed complexes, with ΔE_{ads} = −2.7 kcal· mol^{-1}.

2.3. Trends of the Adsorption Energies

Although the obtained adsorption energies have been commented on in the previous sections, we find it appropriate to dedicate this section to summarize them and highlight the general trends. Figure 6 shows a representation of the ΔE_{ads} values as a function of the type of BNNT for each molecule.

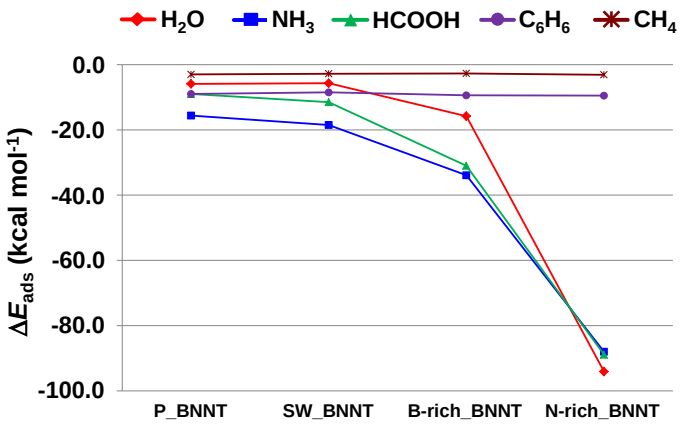

Figure 6. Variation of the adsorption energies (ΔE_{ads}) for the different probe molecules as a function of the BNNTs.

The interaction of the polar molecules with defective BNNTs mostly takes place through dative covalent bonds (the exception is the SW_BNNT/H_2O adduct), while, for the non-polar molecules, the adsorption is dictated by dispersion forces (weaker than dative interactions). Accordingly, polar molecules present larger adsorption energies than non-polar molecules.

Because dative interactions strongly depend on the strength of the direct bond established between the interacting partners, which, in turn, depends on the bonding atoms, for those adducts based on these interactions, the calculated ΔE_{ads} values present large variations as a function of the type of defective BNNT. This varies from those systems based on dispersion interactions and accordingly their calculated ΔE_{ads} values remain almost constant for a given non-polar molecule irrespective of the type of BNNT; namely, between -8.5 and -9.5 kcal mol^{-1} for C_6H_6, and between -2.7 and -3.1 kcal mol^{-1} for CH_4.

Taking only the interaction of the polar molecules with the different BNNTs into account, the trend of the ΔEads values as a function of the type of BNNT is in general (from more to less favorable): N-rich_BNNT > B-rich_BNNT > SW_BNNT > P_BNNT, whereas as a function of the polar molecules is: NH_3 > HCOOH > H_2O. The first trend clearly indicates that the presence of defects at the BNNT walls enhances the interaction with these molecules. Moreover, among the defective BNNTs considered here, those presenting a boron monovacancy are the most reactive ones towards the polar molecules. This is consistent with the fact that the interaction of the polar molecules with N-rich_BNNT, a spontaneous deprotonation, is given for all cases. The second trend indicates that, in general, the adsorption of NH_3 gives the most stable adducts. This is because the dative $B_{(BNNT)}\cdots N_{(NH3)}$ bonds are very stable. However, it is worth highlighting that the largest and most negative ΔE_{ads} values calculated in this work is associated with the N-rich_BNNT/H_2O complex. In this case, H_2O becomes deprotonated upon adsorption and the $B_{(BNNT)}\cdots OH^-$ bond, in addition to being very stable, electrostatic interactions are also operating, which further stabilize the adduct.

3. Computational Details

All calculations were carried out using the periodic *abinitio* code CRYSTAL09 [27]. All the self-consistent field (SCF) calculations and geometry optimizations, which include both lattice parameters and internal atomic coordinates, were performed using the B3LYP-D2* density functional

method. It includes an empirical *a posteriori* correction term proposed by Grimme [28] to account for dispersion forces (missed in the pure B3LYP [29,30] method), but whose initial parameterization (D2) was modified for extended systems (D2*) [31], providing accurate results for the calculations of cohesive energies of molecular crystals and of adsorption processes within a periodic treatment [31–33]. The adopted Gaussian functions consisted of an all electron triple-ζ 6-311G* standard basis set for the B and N atoms of the BNNTs and a TZP basis set from Ahlrichs and coworkers [34] for the probe molecules. This basis set combination has been proven to exhibit small basis set superposition error adsorption energies [24,32].

The shrinking factor of the reciprocal space net defining the mesh of k points in the irreducible Brillouin zone was set to 5, which requires diagonalizing the Hamiltonian matrix in 3 k points [35]. The accuracy of both Coulomb and exchange series was set to values of overlap integrals of 10^{-7} and 10^{-16}, respectively, which ensure a very good numerical accuracy. A pruned (75,974) grid has been used for the Gauss–Legendre and Lebedev quadrature schemes in the evaluation of functionals. The condition to achieve SCF convergence between two subsequent cycles was set to 10^{-7} Hartrees. Full relaxations have been carried out by means of analytical energy gradients [36–38]. Geometry optimizations were performed by means of a quasi-Newton algorithm, in which the quadratic step (BFGS Hessian updating scheme) is combined with a linear one (parabolic fit) [39].

The adsorption energies (ΔE_{ads}) per unit cell of the probe molecules with the BNNTs were computed as:

$$\Delta E_{\mathrm{ads}} = E(SM) - E(S) - E_{\mathrm{m}}(M), \quad (1)$$

where E(SM) is the energy of a fully relaxed unitary cell containing the boron nitride nanotubes S in interaction with the probe molecules M, E(S) is the energy of a fully relaxed unitary cell of the BNNTs alone, and E_m(M) is the molecular energy of the free fully optimized probe molecules. Because dispersion is included during the geometry optimization as a correction term, the total energy E of a given system is defined as:

$$\mathrm{E} = \mathrm{U} + \mathrm{E_D}, \quad (2)$$

where U is the potential energy, which includes the electronic terms (*i.e.*, kinetic energies of the electrons, the attraction of the electrons to the nuclei, and the interelectronic repulsions) and the nuclear−nuclear repulsions, and E_D is the dispersion energy. By introducing expression 2 into expression 1 for each system, the adsorption energy can be rewritten as:

$$\Delta E_{\mathrm{ads}} = \Delta U + \Delta E_{\mathrm{D}}, \quad (3)$$

where ΔU is the contribution of the potential energy in the adsorption, and ΔE_D the contribution of dispersion in the adsorption, that is

$$\Delta U = U(SM) - U(S) - U_{\mathrm{m}}(M), \quad (4)$$

$$\Delta E_{\mathrm{D}} = E_{\mathrm{D}}(SM) - E_{\mathrm{D}}(S) - E_{\mathrm{D,m}}(M). \quad (5)$$

4. Conclusions

Periodic quantum mechanical calculations have been used to simulate the adsorption of H_2O, NH_3 and HCOOH (as probe polar molecules) and C_6H_6 and CH_4 (as probe non-polar molecules) on different zig-zag (6,0) single-walled boron nitride nanotubes (BNNTs) that are defect-free (P_BNNT) or defective BNNTs based on B (N-rich_BNNT) and N (B-rich_BNNT) monovacancies and on Stone-Wales defects (SW_BNNT), with the aim of determining the influence of nanotube defects in the adsorption energies. These calculations are based on the B3LYP-D2* method, which includes the B3LYP hybrid functional with a revised version of the empirical *a posteriori* correction term (D2*) to account for dispersion interactions. The most interesting points emerging from this work are as follows:

(i) Adsorption of polar molecules (with lone pair electrons) on the defective BNNTs is in general dictated by dative interactions established between the electron donor atoms of the molecules and the B atoms of the BNNTs, which produce large charge transfers from the molecules to the BNNT. Such transfers increase the acidity of the polar molecules and the basicity of the N atoms of the BNNTs in such a way that significant H-bond interactions are also established. On the N-rich_BNNT, which presents an N atom fully exposed to the surfaces as a consequence of the B monovacancy, the increase of acidity promotes proton transfers to this N atom, thus forming ion pair adducts. This deprotonation also occurs for the adsorption of HCOOH on the B-rich_BNNT.

(ii) For the polar molecules, the strength of their chemisorption strongly depends on the type of the nanotube and the class of the molecule. General trends on the calculated adsorption energies (from more to less favorable) are, as a function of the type of BNNT: N-rich_BNNT > B-rich_BNNT > SW_BNNT > P_BNNT; and as a function of the class of the polar molecule: NH_3 > HCOOH > H_2O. However, the most stable adduct found in this work is that for H_2O interacting with N-rich_BNNT due to the very stable $B\cdots OH^-$ chemical bond.

(iii) C_6H_6 and CH_4 are physisorbed on the different BNNTs, mainly governed by π-stacking (C_6H_6) and CH-π (CH_4) dispersion interactions. For each molecule, the magnitude of the adsorption energies does not depend on the type of BNNT and accordingly they are almost constant, C_6H_6 being more favorable than for CH_4 (about -9 kcal mol^{-1} and -3 kcal mol^{-1}, respectively).

Since the properties of BNNTs, in particular the band gap, are basically independent of tube morphology and chirality, we expect similar results for other types of BNNTs. That is, the presence of SW defects in armchair (n,n) and chiral BNNTs will expectedly induce a slight reduction of the band gap, and B and N monovacancies will convert them as metallic BNNTs. Moreover, since the wall defects presented in this work are essentially point defects, we also expect similar behavior in the adsorption features of polar and non-polar molecules on armchair (n,n) and chiral BNNTs of similar size and radius.

The results presented here are evidence that adsorption properties of BNNTs can be significantly modulated by the presence of structural defects, in particular those concerning the adsorption of polar protic molecules. This is relevant considering that adsorption on SW_BNNTs induce a decrease of its band gap and that N-rich_BNNT and B-rich_BNNT are found to be metallic, so that they can be of interest for nanoelectro-optical applications.

Acknowledgments: Financial support from MINECO (CTQ2014-60119-P and CTQ2015-62635-ERC) and DIUE (project 2014SGR482) is gratefully acknowledged. Albert Rimola is indebted to Programa Banco de Santander for a UAB distinguished postdoctoral research contract.

Author Contributions: Oriol Matarín performed the simulations; Albert Rimola supervised the simulations and wrote the paper.

Conflicts of Interest: The authors declare no conflict of interest. The founding sponsors had no role in the design of the study; in the collection, analyses, or interpretation of data; in the writing of the manuscript, and in the decision to publish the results.

References

1. Rubio, A.; Corkill, J.L.; Cohen, M.L. Theory of graphitic boron nitride nanotubes. *Phys. Rev. B* **1994**, *49*, 5081–5084. [CrossRef]
2. Blase, X.; Rubio, A.; Louie, S.G.; Cohen, M.L. Stability and Band Gap Constancy of Boron Nitride Nanotubes. *Europhys. Lett.* **1994**, *28*, 335–340. [CrossRef]
3. Chopra, N.G.; Luyken, R.J.; Cherrey, K.; Crespi, V.H.; Cohen, M.L.; Louie, S.G.; Zettl, A. Boron Nitride Nanotubes. *Science* **1995**, *269*, 966–967. [CrossRef] [PubMed]
4. Zhi, C.; Bando, Y.; Tang, C.; Honda, S.; Kuwahara, H.; Golberg, D. Boron nitride nanotubes/polystyrene composites. *J. Mater. Res.* **2006**, *21*, 2794–2800. [CrossRef]

5. Zhi, C.; Bando, Y.; Terao, T.; Tang, C.; Kuwahara, H.; Golberg, D. Towards Thermoconductive, Electrically Insulating Polymeric Composites with Boron Nitride Nanotubes as Fillers. *Adv. Funct. Mater.* **2009**, *19*, 1857–1862. [CrossRef]
6. Sun, Q.; Li, Z.; Searles, D.J.; Chen, Y.; Lu, G.; Du, A. Charge-Controlled Switchable CO_2 Capture on Boron Nitride Nanomaterials. *J. Am. Chem. Soc.* **2013**, *135*, 8246–8253. [CrossRef] [PubMed]
7. Reddy, A.L.M.; Tanur, A.E.; Walker, G.C. Synthesis and hydrogen storage properties of different types of boron nitride nanostructures. *Int. J. Hydrog. Energy* **2010**, *35*, 4138–4143. [CrossRef]
8. Golberg, D.; Bando, Y.; Tang, C.C.; Zhi, C.Y. Boron Nitride Nanotubes. *Adv. Mater.* **2007**, *19*, 2413–2432. [CrossRef]
9. Golberg, D.; Bando, Y.; Huang, Y.; Terao, T.; Mitome, M.; Tang, C.; Zhi, C. Boron Nitride Nanotubes and Nanosheets. *ACS Nano* **2010**, *4*, 2979–2993. [CrossRef] [PubMed]
10. Lin, Y.; Connell, J.W. Advances in 2D boron nitride nanostructures: Nanosheets, nanoribbons, nanomeshes, and hybrids with graphene. *Nanoscale* **2012**, *4*, 6908–6939. [CrossRef] [PubMed]
11. Stone, A.J.; Wales, D.J. Theoretical studies of icosahedral C60 and some related species. *Chem. Phys. Lett.* **1986**, *128*, 501–503. [CrossRef]
12. Zobelli, A.; Ewels, C.P.; Gloter, A.; Seifert, G.; Stephan, O.; Csillag, S.; Colliex, C. Defective Structure of BN Nanotubes: From Single Vacancies to Dislocation Lines. *Nano Lett.* **2006**, *6*, 1955–1960. [CrossRef] [PubMed]
13. Miyamoto, Y.; Rubio, A.; Berber, S.; Yoon, M.; Tománek, D. Spectroscopic characterization of Stone-Wales defects in nanotubes. *Phys. Rev. B* **2004**, *69*, 121413. [CrossRef]
14. Schmidt, T.M.; Baierle, R.J.; Piquini, P.; Fazzio, A. Theoretical study of native defects in BN nanotubes. *Phys. Rev. B* **2003**, *67*, 113407. [CrossRef]
15. Shevlin, S.A.; Guo, Z.X. Hydrogen sorption in defective hexagonal BN sheets and BN nanotubes. *Phys. Rev. B* **2007**, *76*, 024104. [CrossRef]
16. Kang, H.S. Theoretical Study of Boron Nitride Nanotubes with Defects in Nitrogen-Rich Synthesis. *J. Phys. Chem. B* **2006**, *110*, 4621–4628. [CrossRef] [PubMed]
17. Li, Y.; Zhou, Z.; Golberg, D.; Bando, Y.; Schleyer, P.v.R.; Chen, Z. Stone−Wales Defects in Single-Walled Boron Nitride Nanotubes: Formation Energies, Electronic Structures, and Reactivity. *J. Phys. Chem. C* **2008**, *112*, 1365–1370. [CrossRef]
18. An, W.; Wu, X.; Yang, J.L.; Zeng, X.C. Adsorption and Surface Reactivity on Single-Walled Boron Nitride Nanotubes Containing Stone−Wales Defects. *J. Phys. Chem. C* **2007**, *111*, 14105–14112. [CrossRef]
19. Chen, W.; Li, Y.; Yu, G.; Zhou, Z.; Chen, Z. Electronic Structure and Reactivity of Boron Nitride Nanoribbons with Stone-Wales Defects. *J. Chem. Theory Comput.* **2009**, *5*, 3088–3095. [CrossRef] [PubMed]
20. Zhao, J.X.; Ding, Y.H. Theoretical investigation of the divacancies in boron nitride nanotubes: Properties and surface reactivity toward various adsorbates. *J. Chem. Phys.* **2009**, *131*, 014706. [CrossRef] [PubMed]
21. Chen, Y.; Hu, C.L.; Li, J.Q.; Jia, G.X.; Zhang, Y.F. Theoretical study of O_2 adsorption and reactivity on single-walled boron nitride nanotubes. *Chem. Phys. Lett.* **2007**, *449*, 149–154. [CrossRef]
22. Piquini, P.; Baierle, R.J.; Schmidt, T.M.; Fazzio, A. Formation energy of native defects in BN nanotubes: An ab initio study. *Nanotechnology* **2005**, *16*, 827. [CrossRef]
23. Bettinger, H.F.; Dumitrică, T.; Scuseria, G.E.; Yakobson, B.I. Mechanically induced defects and strength of BN nanotubes. *Phys. Rev. B* **2002**, *65*, 041406. [CrossRef]
24. Rimola, A.; Sodupe, M. Physisorption *vs.* chemisorption of probe molecules on boron nitride nanomaterials: The effect of surface curvature. *Phys. Chem. Chem. Phys.* **2013**, *15*, 13190–13198. [CrossRef] [PubMed]
25. Rimola, A.; Sodupe, M. Gas-Phase and Microsolvated Glycine Interacting with Boron Nitride Nanotubes. A B3LYP-D2* Periodic Study. *Inorganics* **2014**, *2*, 334–350. [CrossRef]
26. Rimola, A. Intrinsic Ladders of Affinity for Amino-Acid-Analogues on Boron Nitride Nanomaterials: A B3LYP-D2* Periodic Study. *J. Phys. Chem. C* **2015**, *119*, 17707–17717. [CrossRef]
27. Dovesi, R.; Saunders, V.R.; Roetti, C.; Orlando, R.; Zicovich-Wilson, C.M.; Pascale, F.; Civalleri, B.; Doll, K.; Harrison, N.M.; Bush, I.J.; *et al. CRYSTAL09 User's Manual*; University of Torino: Torino, Italy, 2009.
28. Grimme, S. Semiempirical GGA-type density functional constructed with a long-range dispersion correction. *J. Comput. Chem.* **2006**, *27*, 1787–1799. [CrossRef] [PubMed]
29. Becke, A.D. Density-functional thermochemistry. III. The role of exact exchange. *J. Chem. Phys.* **1993**, *98*, 5648–5652. [CrossRef]

30. Lee, C.; Yang, W.; Parr, R.G. Development of the Colle-Salvetti correlation-energy formula into a functional of the electron density. *Phys. Rev. B* **1988**, *37*, 785–789. [CrossRef]
31. Civalleri, B.; Zicovich-Wilson, C.M.; Valenzano, L.; Ugliengo, P. B3LYP augmented with an empirical dispersion term (B3LYP-D*) as applied to molecular crystals. *CrystEngComm* **2008**, *10*, 405–410. [CrossRef]
32. Rimola, A.; Civalleri, B.; Ugliengo, P. Physisorption of aromatic organic contaminants at the surface of hydrophobic/hydrophilic silica geosorbents: A B3LYP-D modeling study. *Phys. Chem. Chem. Phys.* **2010**, *12*, 6357–6366. [CrossRef] [PubMed]
33. Civalleri, B.; Maschio, L.; Ugliengo, P.; Zicovich-Wilson, C.M. Role of dispersive interactions in the CO adsorption on MgO (001): Periodic B3LYP calculations augmented with an empirical dispersion term. *Phys. Chem. Chem. Phys.* **2010**, *12*, 6382–6386. [CrossRef] [PubMed]
34. Schafer, A.; Horn, H.; Ahlrichs, R. Fully optimized contracted Gaussian basis sets for atoms Li to Kr. *J. Chem. Phys.* **1992**, *97*, 2571–2577. [CrossRef]
35. Monkhorst, H.J.; Pack, J.D. Special points for Brillouin-zone integrations. *Phys. Rev. B* **1976**, *13*, 5188–5192. [CrossRef]
36. Doll, K. Implementation of analytical Hartree–Fock gradients for periodic systems. *Comput. Phys. Commun.* **2001**, *137*, 74–88. [CrossRef]
37. Doll, K.; Dovesi, R.; Orlando, R. Analytical Hartree–Fock gradients with respect to the cell parameter for systems periodic in three dimensions. *Theor. Chem. Acc.* **2004**, *112*, 394–402. [CrossRef]
38. Doll, K.; Saunders, V.R.; Harrison, N.M. Analytical Hartree–Fock gradients for periodic systems. *Int. J. Quantum Chem.* **2001**, *82*, 1–13. [CrossRef]
39. Civalleri, B.; D'Arco, P.; Orlando, R.; Saunders, V.R.; Dovesi, R. Hartree-Fock geometry optimisation of periodic systems with the CRYSTAL code. *Chem. Phys. Lett.* **2001**, *348*, 131–138. [CrossRef]